Antireflection-enhanced color by a natural graded refractive index (GRIN) structure

Chad M. Eliason[1,*] and Matthew D. Shawkey[1]

[1]*Department of Biology and Integrated Bioscience Program, The University of Akron, Akron, OH USA*
[*]*cme16@zips.uakron.edu*

Abstract: Nanostructured materials like graded refractive index (GRIN) structures in moth eyes have inspired the design of novel antireflective coatings. Such structures are more flexible than uniform coatings, but applications have been mainly limited to broadband antireflection in solar cells and LEDs. Here we show that cylindrical pigment granules in two bird species (*Polyplectron bicalcaratum* and *Patagioenas fasciata*) form a GRIN that suppresses interference and expands the range of colors produced by a multilayer. These results demonstrate that a GRIN structure can function like a pigment (i.e. through selective, independent wavelength blocking) to generate unique colors and may inspire the design of novel antireflective and structurally colored coatings.

OCIS codes: (310.1210) Antireflection coatings; (310.6860) Thin films, optical properties; (330.1690) Color; (160.1435) Biomaterials.

References and links

1. S. Kinoshita, *Structural Colors in the Realm of Nature* (World Scientific, 2008), pp. 1–367.
2. I. Newton, *Opticks* (Dover Publications, 1704).
3. J. Grandidier, R. A. Weitekamp, M. G. Deceglie, D. M. Callahan, C. Battaglia, C. R. Bukowsky, C. Ballif, R. H. Grubbs, and H. A. Atwater, "Solar cell efficiency enhancement via light trapping in printable resonant dielectric nanosphere arrays," Phys. Status Solidi A **210**(2), 255–260 (2013).
4. C.-Y. Fang, Y.-L. Liu, Y.-C. Lee, H.-L. Chen, D.-H. Wan, and C.-C. Yu, "Nanoparticle Stacks with Graded Refractive Indices Enhance the Omnidirectional Light Harvesting of Solar Cells and the Light Extraction of Light-Emitting Diodes," Adv. Funct. Mater. **23**(11), 1412–1421 (2013).
5. E. Hecht and A. Zajac, *Optics*, 4 ed. (Addison Wesley, 2002).
6. E. F. Schubert, J. K. Kim, and J.-Q. Xi, "Low-refractive-index materials: A new class of optical thin-film materials," Phys. Status Solidi B **244**(8), 3002–3008 (2007).
7. S. J. Wilson and M. C. Hutley, "The optical properties of moth eye antireflection surfaces," J. Mod. Opt. **29**, 993–1009 (1982).
8. J.-Q. Xi, M. F. Schubert, J. K. Kim, E. F. Schubert, M. Chen, S.-Y. Lin, W. Liu, and J. A. Smart, "Optical thin-film materials with low refractive index for broadband elimination of Fresnel reflection," Nat. Photonics **1**, 176–179 (2007).
9. H. Durrer, ""Schillerfarben der vogelfeder als evolutionsproblem," Denkschr. Schweiz," Naturf. Ges. **91**, 1–127 (1977).
10. R. O. Prum, "Anatomy, physics, and evolution of structural colors," in *Bird Coloration, Vol. I*, Mcgraw, K. J. and Hill, G. E., eds. (Harvard Univ. Press, 2006), Vol. 1, pp. 295–353.
11. D. G. Stavenga, B. D. Wilts, H. L. Leertouwer, and T. Hariyama, "Polarized iridescence of the multilayered elytra of the Japanese jewel beetle, Chrysochroa fulgidissima," Philos. Trans. Roy. Soc. Lond. B Biol. Sci. **366**(1565), 709–723 (2011).
12. M. D. Shawkey, A. M. Estes, L. M. Siefferman, and G. E. Hill, "Nanostructure predicts intraspecific variation in ultraviolet-blue plumage colour," Proc. Biol. Sci. **270**(1523), 1455–1460 (2003).
13. M. D. Abràmoff, P. J. Magalhães, and S. J. Ram, "Image processing with ImageJ," Biophoton. Int. **11**, 36–42 (2004).
14. R. Maia, C. M. Eliason, P.-P. Bitton, S. M. Doucet, and M. D. Shawkey, "pavo: an R package for the analysis, visualization and organization of spectral data," Methods Ecol. Evol. **4**, 906–913 (2013).
15. R. Diamant, A. Garcí-Valenzuela, and M. Fernández-Guasti, "Reflectivity of a disordered monolayer estimated by graded refractive index and scattering models," J. Opt. Soc. Am. A **29**(9), 1912–1921 (2012).
16. B. Q. Dong, X. H. Liu, T. R. Zhan, L. P. Jiang, H. W. Yin, F. Liu, and J. Zi, "Structural coloration and photonic pseudogap in natural random close-packing photonic structures," Opt. Express **18**(14), 14430–14438 (2010).

#202919 - $15.00 USD Received 11 Dec 2013; revised 28 Feb 2014; accepted 3 Mar 2014; published 19 Mar 2014

17. M. Skoge, A. Donev, F. H. Stillinger, and S. Torquato, "Packing hyperspheres in high-dimensional Euclidean spaces," Phys. Rev. E Stat. Nonlin. Soft Matter Phys. **74**(4), 041127 (2006).
18. G. Jellison, Jr., "Data analysis for spectroscopic ellipsometry," Thin Solid Films **234**(1-2), 416–422 (1993).
19. A. Oskooi, D. Roundy, M. Ibanescu, P. Bermel, J. Joannopoulos, and S. Johnson, "MEEP: A flexible free-software package for electromagnetic simulations by the FDTD method," Comput. Phys. Commun. **181**(3), 687–702 (2010).
20. D. Brink and N. van der Berg, "Structural colours of the bird *Bostrychia hagedash*," J. Phys. D Appl. Phys. **37**(5), 813–818 (2004).
21. J. Zi, X. Yu, Y. Li, X. Hu, C. Xu, X. Wang, X. Liu, and R. Fu, "Coloration strategies in peacock feathers," Proc. Natl. Acad. Sci. U.S.A. **100**(22), 12576–12578 (2003).
22. H. L. Leertouwer, B. D. Wilts, and D. G. Stavenga, "Refractive index and dispersion of butterfly chitin and bird keratin measured by polarizing interference microscopy," Opt. Express **19**(24), 24061–24066 (2011).
23. S. S. Yoshioka and S. S. Kinoshita, "Direct determination of the refractive index of natural multilayer systems," Phys. Rev. E Stat. Nonlin. Soft Matter Phys. **83**(5), 051917 (2011).
24. M. Vorobyev, D. Osorio, A. T. D. Bennett, N. J. Marshall, and I. C. Cuthill, "Tetrachromacy, oil droplets and bird plumage colours," J. Comp. Physiol. A Neuroethol. Sens. Neural Behav. Physiol. **183**(5), 621–633 (1998).
25. J. A. Endler and P. Mielke, Jr., "Comparing entire colour patterns as birds see them," Biol. J. Linn. Soc. Lond. **86**(4), 405–431 (2005).
26. S. C. Lee, "Dependent scattering of an obliquely incident plane wave by a collection of parallel cylinders," J. Appl. Phys. **68**(10), 4952–4957 (1990).
27. B. E. Perilloux, *Thin-Film Design: Modulated Thickness and Other Stopband Design Methods* (SPIE Press, 2002).
28. S. Orfanidis, *Electromagnetic Waves and Antennas*; available at http://www.ee.rutgers.edu/orfanidi/ewa/ (last accessed June 2013).
29. E. Nakamura, S. Yoshioka, and S. Kinoshita, "Structural Color of Rock Dove's Neck Feather," J. Phys. Soc. Jpn. **77**(12), 124801 (2008).
30. M. D. Shawkey, L. D'Alba, J. Wozny, C. M. Eliason, J. A. H. Koop, and L. Jia, "Structural color change following hydration and dehydration of iridescent mourning dove (Zenaida macroura) feathers," Zoology (Jena) **114**(2), 59–68 (2011).
31. Q. Yang, X. A. Zhang, A. Bagal, W. Guo, and C.-H. Chang, "Antireflection effects at nanostructured material interfaces and the suppression of thin-film interference," Nanotechnology **24**(23), 235202 (2013).
32. J. H. Noh, S. H. Im, J. H. Heo, T. N. Mandal, and S. I. Seok, "Chemical management for colorful, efficient, and stable inorganic-organic hybrid nanostructured solar cells," Nano Lett. **13**(4), 1764–1769 (2013).
33. M. Li, L. Zeng, Y. Chen, L. Zhuang, X. Wang, and H. Shen, "Realization of Colored Multicrystalline Silicon Solar Cells with SiO 2/SiN x: H Double Layer Antireflection Coatings," Int. J. Photoenergy **2013**, 1–8 (2013).
34. R. Maia, R. H. F. Macedo, and M. D. Shawkey, "Nanostructural self-assembly of iridescent feather barbules through depletion attraction of melanosomes during keratinization," J. R. Soc. Interface **9**(69), 734–743 (2012).
35. K. J. M. Bishop, C. E. Wilmer, S. Soh, and B. A. Grzybowski, "Nanoscale forces and their uses in self-assembly," Small **5**(14), 1600–1630 (2009).
36. M. Nolte, I. Dönch, and A. Fery, "Freestanding polyelectrolyte films as sensors for osmotic pressure," ChemPhysChem **7**(9), 1985–1989 (2006).
37. M. L. Bruening, D. M. Dotzauer, P. Jain, L. Ouyang, and G. L. Baker, "Creation of functional membranes using polyelectrolyte multilayers and polymer brushes," Langmuir **24**(15), 7663–7673 (2008).

1. Introduction

Multilayers produce structural colors through constructive interference of light beams reflecting at different interfaces. The reflectance of such structures is determined by the number of layers, refractive index (RI) contrast between layers, thicknesses of individual layers, and the polarization and angle of incident light [1]. Reflectance maxima (λ_{max}) for a simple 2-layer stack can be determined using the Bragg-Snell diffraction equation [1]:

$$(m-1/2)\lambda_{\max} = 2\left(d_1\sqrt{n_1^2-\sin^2\theta}+d_2\sqrt{n_2^2-\sin^2\theta}\right) \quad (1)$$

where n and d are the RIs and thicknesses of the two layers, m is the diffraction order, and θ is the incident angle of light. Because numerous wavelengths fulfill the condition for diffraction (i.e. multiple values of m), reflectance spectra produced by such structures are often multi-peaked in visible wavelengths. Newton first observed that the series of colors produced by thin films of increasing thickness were not monochromatic but "compound," and thus unsaturated [2]. Achieving more saturated colors requires either an increase in the number of layers [1] or narrowband reduction of reflection at an interface.

#202919 - $15.00 USD Received 11 Dec 2013; revised 28 Feb 2014; accepted 3 Mar 2014; published 19 Mar 2014

Controlling reflection at the interface between two materials differing in RI is important for a wide variety of industrial applications like solar cells [3,4] and LED light extraction [4]. One common control mechanism is a thin-film coating with quarter-wavelength thickness and a RI of $\sqrt{n_0 n_{sub}}$, where n_0 and n_{sub} are the RIs of the ambient material and substrate, respectively [5]. However, no materials that form films have RIs less than ~1.4, limiting the flexibility of this method [6]. Alternatively, materials could be structured to produce a graded refractive index (GRIN), in which RI varies gradually and consistently throughout the nanostructure. Because Fresnel reflection depends on RI contrast at an interface, such incremental steps in RI can strongly reduce reflection, as in the antireflecting bumps on the surface of moth eyes [7]. Inspired by these natural structures, researchers have recently achieved RIs approaching that of air (n = 1.00), strongly reducing Fresnel reflection over a range of wavelengths and incident angles [8].

Birds have evolved diverse photonic structures (e.g., multilayers, photonic crystals, thin films) [9,10] from relatively few materials (keratin, melanin and air) [10]. Despite this material limitation, the often non-planar shapes of melanin-containing organelles (melanosomes) might produce a GRIN (e.g., see [11]), potentially reducing interference and enhancing color. Here, we test this hypothesis in two bird species: the grey peacock-pheasant (*Polyplectron bicalcaratum*) and the band-tailed pigeon (*Patagioenas fasciata*). Using a combination of electron microscopy, reflectance spectrometry, focused ion beam (FIB) milling, and optical modeling, we show that iridescent color is caused by interference from a composite structure consisting of a uniform keratin layer and a monolayer of cylindrical melanosomes. Structural analyses and optical simulations suggest that melanosomes enhance color by forming a GRIN to reduce reflection at the cortex-melanosome interface and produce a broader gamut of colors than is possible with a non-GRIN structure.

2. Methods

2.1 Morphological analysis

We obtained untreated feathers from private sellers and museum collections (*Patagioenas fasciata*: University of Akron Ornithological Collection #1050; *Polyplectron bicalcaratum*: Field Museum of Natural History, David Willard curator). Peacock-pheasants have numerous iridescent eyespots on their tail and body and we analyzed a contour feather eyespot (Fig. 1(a)). Band-tailed pigeons are generally drab brown except for a yellow iridescent patch on their necks, thus we plucked a feather from this region (Fig. 1(d)). We used TEM to image transverse cross-sections of feathers barbules following the protocol in Shawkey et al. [12]. From the resulting TEM images, we used ImageJ [13] to measure melanosome diameter (d_{mel}) and keratin cortex thickness (d_{ker}) thickness at haphazardly chosen locations along the exposed surface of a barbule. To confirm that melanosomes were surrounded by air as previously suggested [9], we used a dual-beam FIB (Nova Nano-lab 200, FEI, Hillsboro, OR, USA) at an operating voltage of 30kV and a current of 0.8 nA to ablate the entire cortex and leave the underlying melanosomes intact.

2.2 Spectral analysis

We measured angle-resolved spectra (from 10 to 70° in 5° increments) at two incident light polarizations (*s*: E-field parallel to surface; *p*: E-field perpendicular to surface) using a linear grid polarizer (Thorlabs, Newton, NJ, USA) placed between the light source and feather. We mounted feathers so that the reflecting structures (barbules) were oriented perpendicular to the incident light on a lab-made goniometer. From the measured curves, we calculated the location (λ_{max}) and amplitude of reflectance peaks (R_{max}) using the R package pavo [14].

#202919 - $15.00 USD Received 11 Dec 2013; revised 28 Feb 2014; accepted 3 Mar 2014; published 19 Mar 2014

2.3 Optical modeling

To understand the structural color mechanism, we compared the match between measured and predicted reflectance spectra for two different structural models based on previous studies and TEM measurements: 1) a keratin thin film over a melanosome layer with a GRIN [15]; and 2) a keratin thin film over a melanosome monolayer and amorphous melanosome substrate [16]. For model 1 we calculated RI as a function of vertical position by dividing the melanosome layer into vertical slices and homogenizing their refractive indices according to the proportions of melanin and air. Based on similar equations in for spheres [15], the refractive index as a function of depth into the cylinder (z) is:

$$n(z) = n_{\text{air}} + \frac{\Theta}{r}\left(n_{\text{mel}} - n_{\text{air}}\right)\sqrt{-z^2 - 2zr} \qquad (2)$$

where n_{air} = 1.00, n_{mel} = 2.00, r is the melanosome radius and Θ is the ratio of melanosome diameter to space between melanosomes (Θ = 0 refers to melanosomes with infinite space between them and Θ = 1 to close-packed melanosomes). We determined Θ ≈0.75 from TEM measurements. There was a good match between predicted $n(z)$ and empirical variation in average grey value with position along the z-axis through a melanosome monolayer (Fig. 1(f)). For model 2, we used a molecular dynamics, collision-based simulation algorithm to generate random melanosome packing configurations [17] similar to those observed in feathers. To evaluate the match between real and simulated structures, we compared radial distribution functions for the simulated and empirical structures using the x and y coordinates of between 20 and 60 melanosomes per barbule measured from TEM images.

We used the transfer matrix method [18] implemented in an R script to compute reflectance spectra for model 1. To calculate reflectance for model 2 and validate the GRIN method in model 1, we used the finite difference time domain method (FDTD) implemented in Meep [19]. We used published values for the refractive index of melanin (n_{mel} = 2.00) [20,21] and keratin (n_{ker} = 1.56) [22]. The extinction coefficient of avian melanin has not been empirically determined, thus we used a value for a melanin-like material in beetles (k_{mel} = 0.1 at 400 nm) [23].

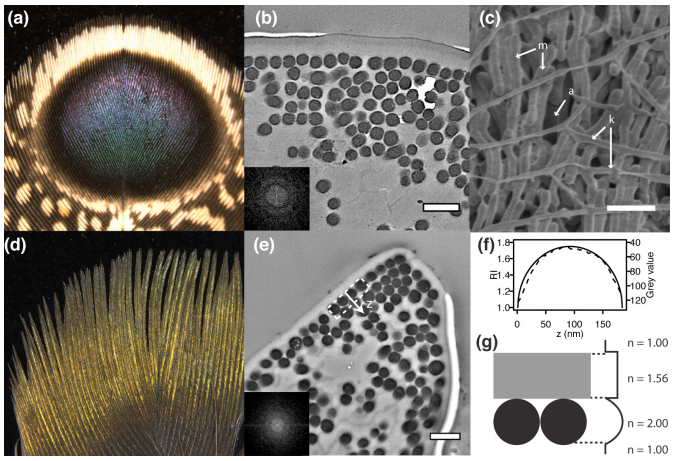

Fig. 1. Color and nanostructure of iridescent feathers. (a,d) Optical images of iridescent feathers from the grey peacock-pheasant (a) and band-tailed pigeon (d). (b,e) TEM images of feather barbule cross-sections; lower insets are FFTs of pictured regions. (c) SEM longitudinal view of melanosomes, with labels indicating melanosomes (*m*), keratin channels (*k*) and air spaces (*a*). (f) Measured average grey value (dashed line) versus z for the boxed region shown in (e) along with refractive index $n(z)$ versus z (solid line) calculated with Eq. (2). (g) Schematic diagram of GRIN model. All scale bars are 500 nm.

#202919 - $15.00 USD Received 11 Dec 2013; revised 28 Feb 2014; accepted 3 Mar 2014; published 19 Mar 2014

2.4 Colorspace analyses

To compare the range of colors produced by GRIN and uniform layers, we converted calculated spectra (without melanin absorption) to Commission Internationale de Eclairage (CIE) *xyY* coordinates following Dong et al. [16] using 1931 CIE color-matching functions obtained from the Color and Vision Research Laboratory. We also converted spectra to *xyz* coordinates using information on the visual physiology of birds. Unlike humans, birds have a fourth UV-sensitive color-sensitive cone in their retina allowing for perception of a broader range of colors (reviewed in [24]). To compare simulated spectra in this avian colorspace, we first computed quantum catches for each cone as $q_i = \sum_{\lambda=300}^{700} R(\lambda)S_i(\lambda)$, where q_i is the amount of light captured by cone *i*, *R* is the reflectance at a given wavelength and *S* is the cone sensitivity [24]. We then converted these q_i values into 3D *xyz* coordinates using published equations [25].

Peak locations depend on optical thickness (*nd*) of a nanostructure. Thus, to control for difference in *n* for GRIN and uniform layers of melanin, we calculated an adjusted melanin layer thickness (d_{adj}) to give equivalent optical thicknesses for the graded and uniform index structures:, $d_{adj} = (n_1 d_1)/n_2$ where $n_1 = 1.59$ and $n_2 = 2.00$.

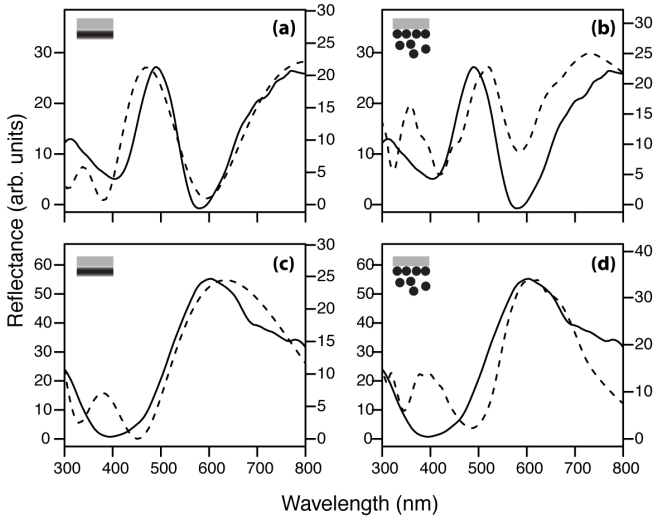

Fig. 2. Match between measured and modeled reflectance spectra in the peacock-pheasant (a,b) and pigeon (c,d). Lines show empirical (solid, y-axis) and predicted reflectance (dashed, secondary y-axis) for candidate optical models. (a,c) Model 1: cortex and graded index melanosome layer. (b,d) Model 2: amorphous melanosome nanostructure. Values used in calculations: $n_{mel} = 2.00$, $n_{air} = 1.00$, $k_{mel} = 0.1$, and $n_{ker} = 1.56$. All models have air as the substrate. Amplitudes of the spectra were adjusted to allow for easier comparison.

3. Results

3.1 Feather nanostructure

In both species, melanosomes formed a loosely-packed monolayer at the edges of barbules (Fig. 1(b), 1(e)) and were surrounded by air (Fig. 1(c)), consistent with previous findings [9]. FFTs of barbule cross-sections showed weak 2D positional ordering of melanosomes (insets in Fig. 1(b), 1(e)). The cylindrical shape of melanosomes produced a GRIN, as indicated by variation in electron density with position as shown in Fig. 1(f). The diameters of melanosomes (d_{mel}) were 145 nm (95% confidence interval, CI: 136-162 nm) and 156 nm (CI: 141-177), and the average keratin cortex thicknesses (d_{ker}) were 242 nm (CI: 222-257 nm) and 155 nm (CI: 138-179 nm) in *Polyplectron* and *Patagioenas*, respectively.

#202919 - $15.00 USD Received 11 Dec 2013; revised 28 Feb 2014; accepted 3 Mar 2014; published 19 Mar 2014

3.2 Spectral analysis

Reflectance spectra measured at near-normal incidence (10°) for *p*- and *s*-polarized incident light were similar, suggesting that the observed orientational disorder of melanosomes in Fig. 1(c) eliminates the linear polarization expected for light scattering from parallel cylinders [26]. There was a good match between the measured and predicted reflectance spectra based on the best-fitting GRIN model (Fig. 2(a), 2(c)). Different levels of k_{mel} (from 0 - 0.3) had only a minor effect on spectral shape; specifically, the small peaks near 350 nm decreased in amplitude relative to the overall spectrum.

Feather color was strongly iridescent in both species and reflectance became more linearly polarized with incident angle (Fig. 3(a), 3(c)), consistent with thin-film optical theory [27] and simulated reflectance data (Fig. 3(b), 3(d)). Angle-resolved results were similar for both species, thus only those for the peacock-pheasant are presented here.

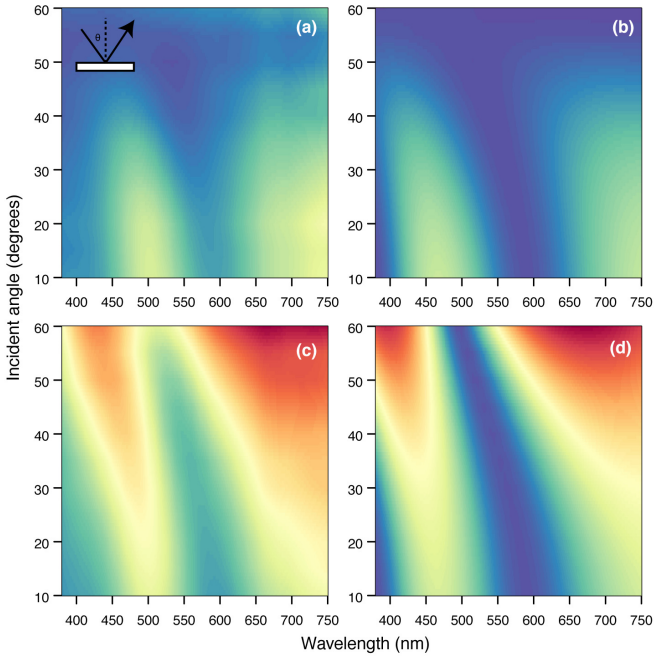

Fig. 3. Measured and calculated changes in reflectance with incident angle for grey peacock-pheasant feathers. False color maps showing measured (a,c) and calculated (b,d) reflectance versus wavelength and incident angle (blue: minimum, red: maximum). Upper panels are results for light polarized perpendicular to melanosomes (*p*-polarization) and lower panels are with light polarized parallel to melanosomes (*s*-polarization). Schematic shows optical setup (white rectangle: feather surface, black arrows: light direction, vertical dashed line: surface normal).

3.3. Antireflection mechanism

To explore the potential antireflection properties of the GRIN layer formed by melanosomes, we simulated reflectance at a keratin-air interface with and without an adjacent GRIN layer. Figure 4(a) shows reflectance as a function of reduced frequency d_{mel}/λ (for comparison of reflectance at different thicknesses and wavelengths) with and without melanin absorption, revealing strong antireflection at multiple frequencies compared to a bare keratin interface (R < 0.05% versus 4.8%). Similar antireflection can also be achieved with a uniform layer, but optical simulations revealed that the GRIN layer functions over a broader range of RIs (R < 0.01% for n = 1.78 - 1.87 compared to 1.24 - 1.26 for a non-GRIN layer) and the optimal RI

#202919 - $15.00 USD Received 11 Dec 2013; revised 28 Feb 2014; accepted 3 Mar 2014; published 19 Mar 2014

was 1.82 compared to 1.25 for a uniform layer, impossible to achieve with available film-forming materials [6].

Next, to understand the link between antireflection at the cortex-GRIN layer interface and color of the composite structure, we simulated reflectance at a reduced frequency of 1.24 but with a finite upper keratin cortex varying in thickness. This frequency was chosen because its antireflection properties were similar for absorbing and non-absorbing cases (arrow in Fig. 4(a)). Figure 4(b) shows that, compared to a uniform layer of melanin, reflectance of a nanostructure with a GRIN layer varies only slightly with phase thickness, $\delta = 2\pi\left(n_{\mathrm{ker}}d_{\mathrm{ker}} + n_{\mathrm{mel}}d_{\mathrm{mel}}\right)/\lambda$, around a mean value of 4.8%. This weak relationship between R and δ indicates that antireflection at the keratin-melanosome interface suppresses interference at specific wavelengths, and that this effect is largely independent of cortex thickness. Thus, color produced by these structures is flexible and maintains constant light transmission over a given wavelength range.

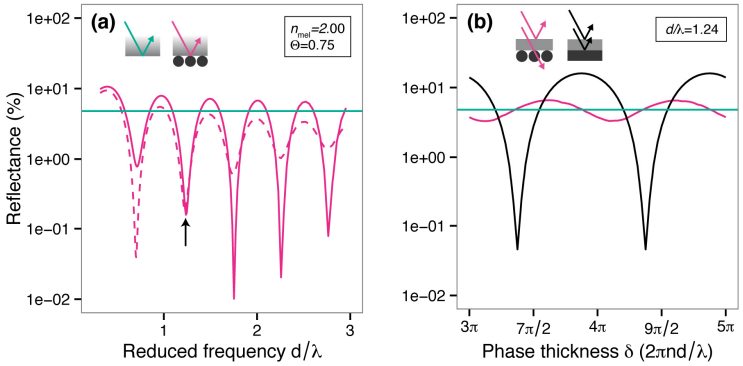

Fig. 4. Antireflection and interference suppression by a GRIN structure. (a) Reflectance versus reduced frequency (d_{mel}/λ) for a GRIN layer under bulk keratin (n_{ker} = 1.56) both without (solid line) and with absorption (dashed line, k_{mel} = 0.1). Horizontal green line is reflectance calculated for a bare keratin-air interface (R = 4.8%). (b) Reflectance versus phase thickness δ at d_{mel}/λ = 1.24 (marked by vertical arrow in (a)) for a GRIN (pink) and uniform (black) composite structure varying in cortex thickness (d_{ker}). Note the log scale for the y-axis.

3.4. Colorspace analysis

Reflectance simulations for the GRIN and uniform melanin layers over a range of parameter combinations for d_{mel} and d_{ker} (both varying from 50 to 450 nm in 10-nm increments) indicated that the range of theoretical colors for a uniform layer is limited relative to a GRIN layer. Figure 5(a) shows that the GRIN layer produces more colors extending further toward the edges of the CIE color gamut (i.e. pure, monochromatic colors). We found a similar pattern for analyses of spectra in avian 3D colorspace (Fig. 5(b)). The color gamut shown in Fig. 5 is for simulations without melanin absorption (k_{mel} = 0) because we wanted to investigate the independent effects of nanostructure on color production. Additional simulations including a wavelength-dependent extinction coefficient for melanin [23] and keratin [22] produced similar results (i.e. more colors were possible with a GRIN layer).

The limited range of colors produced by a layered structure with uniform RI can be understood with wave impedance theory [28]. For a 2-layer stack of non-absorbing uniform layers, a reflectance peak will reach a maximum when the layer thicknesses are λ/2 (high RI) and λ/4 (low RI) and a minimum when the layer thicknesses are λ/4 (low RI) and λ/2 (high RI). The amplitude of the peak is a function of the RI of the layer (n), ambient medium (n_0) and substrate (n_{sub}):

$$R = \left[\left(n^2 - n_0 n_{\mathrm{sub}}\right)/\left(n^2 + n_0 n_{\mathrm{sub}}\right)\right]^2 \qquad (3)$$

#202919 - $15.00 USD Received 11 Dec 2013; revised 28 Feb 2014; accepted 3 Mar 2014; published 19 Mar 2014

Thus, for a uniform stack of keratin (n = 1.56) and melanin (n = 2.00), the amplitude of a reflectance peak can vary from 17.4 - 36.0%, giving a maximum peak height ratio of 2.07. By comparison, peak values for the GRIN layer ranged from ~5 to 25% (maximum peak height ratio ~5), producing greater variation in spectral shape and thus more saturated colors (Fig. 5(a), outsets).

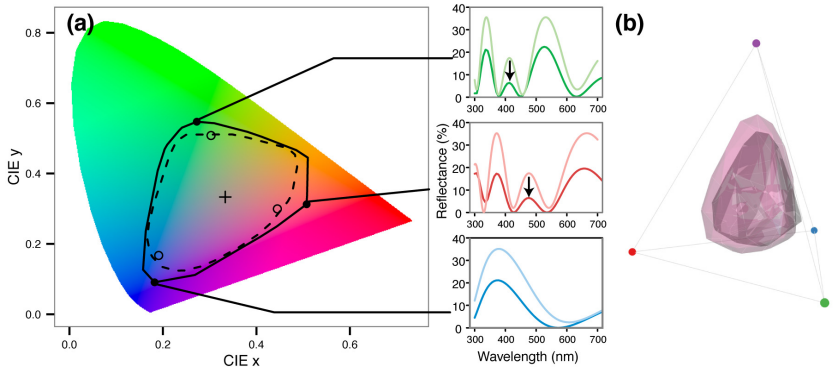

Fig. 5. Colorspace expansion by a GRIN layer. (a) Calculated spectra in CIE colorspace for different combinations of d_{ker} and d_{mel}. Lines are minimum convex polygons enclosing spectra (solid: GRIN, dashed: uniform). Outsets show extreme spectra corresponding to indicated points for GRIN (dark lines, closed circles) and equivalent uniform layers (light lines, open circles) with similar optical thickness and optimized for minimal reflectance (i.e. $n_{ker}d_{ker} = \lambda/4$); vertical arrows correspond to d_{mel}/λ = 1.24 as in Fig. 4(a). (b) Calculated spectra in avian tetrahedral colorspace (pink: GRIN, black: uniform) with vertices corresponding to long- (red), medium- (green), short- (blue) and UV-sensitive cones (violet) in a bird retina. Absorption by melanin was neglected in order to highlight the independent effects of nanostructure on color, and for comparison with Eq. (3) calculations.

4. Discussion

Recent studies on similar structures in closely related rock pigeons and mourning doves indicate that only the cortex is involved in coloration [29,30]. Nakamura et al. [29] suggested this was due to melanosome disorder or size variation. An alternative hypothesis is that the large melanosomes in these species may strongly scatter light in the forward direction, decoupling the optical effects of the cortex and melanosome layers. Consistent with this hypothesis, our simulations for absorbing melanosomes show decreasing variation in reflectance with wavelength at large diameters ($d/\lambda > 3$; Fig. 4(a)), suggesting that large melanosomes play a minimal role in producing interference colors.

Previous morphological data [9] for the two species analyzed here fall within the confidence intervals of our measurements for the peacock-pheasant (d_{mel} = 148 nm, d_{ker} = 245 nm) but not the pigeon (d_{mel} = 192 nm, d_{ker} = 111 nm). This latter disagreement could be due to the fact that we analyzed a different part of the feather barbule (curved, exposed regions compared to flat sides obscured by adjacent barbules in Durrer [9]) or morphological variation between individuals. Interestingly, the total thickness ($d_{mel} + d_{ker}$) of the composite structures were comparable (303 nm in Durrer compared to 311 nm here), thus the predicted peak locations would be similar.

Similar interference suppression to that shown in Fig. 4(b) has recently been described in artificial materials using nanocone arrays [31]. However, our results differ because the change in RI at the cortex-melanosome interface is abrupt rather than gradual, the melanosome layer has a finite thickness, and the interference reduction is over a narrower range of wavelengths, facilitating more subtle variations in color (Fig. 5(a)). These results suggest a possible route to engineered solar cells with flexible structural colors that maintain constant light transmission over a target wavelength range [32,33].

#202919 - $15.00 USD Received 11 Dec 2013; revised 28 Feb 2014; accepted 3 Mar 2014; published 19 Mar 2014

Color-producing nanostructures in birds likely develop by self-assembly of basic feather materials [34], therefore nanostructural diversity may be driven by variation in basic parameters controlling the self-assembly process. Comparing our morphological results to those of highly ordered photonic crystals in peacocks [21] provides an opportunity to explore potential traits involved in development of disordered and ordered nanostructures. Large colloidal particles like melanosomes typically aggregate into disordered structures unless there is a long-range interaction force stabilizing them [35]. The presence of air between melanosomes observed in Fig. 1(c) likely reduces short-range order (Fig. 1(b), 1(e) insets) and, at the same time, provides a strong RI contrast for saturated colors (Fig. 5(a)). Understanding the development of a keratin cortex over a porous network of melanosomes may also give insight into the design of suspended polymer membranes for applications in pressure sensing [36] or nanofiltration [37].

We have described a composite nanostructure in birds that likely causes suppression of interference and therefore reduction in the secondary reflectance peaks produced by multilayer reflectors. Melanosomes provide a strong RI contrast similar to other natural structures [16], highlighting a largely unexplored gamut of natural materials for novel antireflective and structural color applications. We expect these results will inspire the biomimetic design of non-hazardous and cost-effective LEDs, solar cells, and color displays.

Acknowledgments

We thank L. D'Alba, M. Xiao, D. Fechyr-Lippens, R. Maia, M. Blastrom, B. Hsiung, J. Peteya and an anonymous reviewer for helpful comments and discussion on earlier versions of this manuscript. A. Avishai provided methodological insight and performed FIB-SEM analysis. This work was supported by grants HFSP RGY0083 and AFOSR FA9550-09-1-0159 (both to M.D.S.).